International Journal of Power Electronics and Drive System (IJPEDS)
Vol. 17, No. 4, December 2026, pp. 2770~2780
ISSN: 2088-8694, DOI: 10.11591/ijpeds.v17.i4.pp2770-2780

High-gain single-switch DC–DC converter with incremental conductance MPPT control for fuel cell applications

Thanh-Lam Le, Nguyen Thi Bich Mai
Faculty of Electrical and Electronics Engineering, Ho Chi Minh City University of Technology and Engineering, Ho Chi Minh City, Vietnam

Article Info

Article history:

Received Jul 30, 2026
Revised Sep 17, 2026
Accepted Oct 4, 2026

Keywords:

Energy harvesting
High-gain single-switch DC–DC converter
Incremental conductance MPPT
Proton exchange membrane fuel cell
Voltage regulation

ABSTRACT

An ultra-high-step-up single-switch DC–DC converter is presented for proton exchange membrane fuel cell interfaces that require a regulated high-voltage DC bus from a low and load-dependent source voltage. Its distinguishing feature is the combination of an LCL-type switched-inductor input network and an enhanced quadratic boost stage in a single-switch topology, integrated with incremental-conductance maximum power point tracking (MPPT) and DC-bus regulation. Simulations using a 1.26 kW proton exchange membrane fuel cell (PEMFC) model show conversion from 20 V to a regulated 300 V at approximately 80% efficiency. Under the same source, load, and MPPT conditions, the high-gain single-switch (HGSS) converter delivers about 25% more output power than a conventional boost converter, reduces root mean square (RMS) and peak-to-peak output ripple by approximately 85%, and operates at a duty cycle of 0.52 rather than 0.9. These results identify the topology–control combination as a candidate for high-gain PEMFC interfaces, subject to experimental verification of losses and long-term operation.

This is an open access article under the CC BY-SA license.

Corresponding Author:

Thanh-Lam Le
Faculty of Electrical and Electronics Engineering
Ho Chi Minh City University of Technology and Engineering
Ho Chi Minh City, Vietnam
Email: lamlethanh@hcmute.edu.vn

1. INTRODUCTION

The transition from fossil-based energy systems toward cleaner and more sustainable alternatives has intensified the development of renewable generation and advanced power-electronic interfaces [1], [2]. Proton exchange membrane fuel cells (PEMFCs) are particularly attractive because they directly convert hydrogen into electricity, offer high power density and efficiency, and produce water as the principal reaction product [3]. Their electrical output, however, is characterized by a low and load-dependent terminal voltage. Practical stacks commonly operate at only a few tens of volts, while downstream DC buses, inverters, and distribution loads require substantially higher and tightly regulated voltage levels [4], [5]. Fuel-cell systems may also incorporate batteries or supercapacitors and bidirectional energy-storage interfaces to improve transient power capability, which further increases the importance of coordinated converter and control design [6], [7]. Consequently, a high-gain front-end DC–DC converter with reliable regulation, low source-current ripple, and adequate efficiency is essential for effective PEMFC integration [8].

A conventional boost converter can theoretically provide a large step-up ratio, but the required gain from a low-voltage fuel-cell stack forces the duty cycle close to unity. Under this condition, parasitic resistance, diode reverse recovery, high peak current, and semiconductor voltage stress substantially reduce the practical gain and efficiency [9]. Isolated flyback, push–pull, and related high step-up converters can use

transformer turns ratios to increase the output voltage, but leakage-inductance spikes, bulky magnetic components, and added control and design complexity limit their attractiveness in compact systems [10], [11]. Non-isolated high-gain converters therefore remain a strong alternative. Quadratic, multistage, switched-inductor, switched-capacitor, and voltage-lift structures can extend the conversion ratio at moderate duty cycles and distribute voltage stress among multiple components [5], [12]-[14]. Nevertheless, increased circuit order and additional energy-storage paths introduce stronger dynamic coupling, more design variables, and possible penalties in conduction loss, component count, and transient response.

These trade-offs show that high-gain converter development should not be treated as a topology-only problem. The converter and controller must jointly address voltage amplification, source-current quality, device stress, output regulation, and robustness against input and load variations. Robust proportional–integral–derivative (PID), backstepping sliding-mode, and other nonlinear strategies have improved the regulation of boost-derived converters, while higher-order structures and learning-based control provide additional design possibilities [15]-[18]. For PEMFC sources, input-current ripple is especially important because converter-generated current harmonics interact with the electrochemical dynamics of the stack [19]. Recent studies have therefore emphasized continuous-input-current converter structures, ripple-reduction interfaces, and experimental evaluation of ripple-related degradation [5], [20], [21]. A suitable front-end topology should consequently achieve a high conversion ratio without extreme duty-cycle operation while maintaining a smooth source current and a stable high-voltage output.

Maximum power point tracking (MPPT) is also required because the fuel-cell power–voltage characteristic is nonlinear and varies with operating conditions. Data-driven, hybrid, fractional-order, and intelligent MPPT schemes can improve tracking performance, but they generally require greater computational effort, parameter tuning, or training data [22]-[26]. The perturb and observe (P&O) method is simple, yet its fixed perturbation produces a compromise between tracking speed and steady-state oscillation. Drift-free and soft-tracking variants reduce this limitation but add decision logic or adaptation mechanisms [27], [28]. Incremental conductance (IncCond) determines the operating direction from the power-slope condition and can reduce unnecessary perturbation near the maximum power point (MPP). Enhanced and variable-step IncCond methods have demonstrated improved tracking under changing conditions [29], [30]. Therefore, IncCond offers an appropriate balance among implementation simplicity, tracking accuracy, and computational burden for the proposed fuel-cell interface.

Existing quadratic and switched-inductor converters improve voltage gain at moderate duty cycles, but their use in low-voltage PEMFC interfaces still involves trade-offs among gain, source-current conditioning, device stress, and circuit complexity. To address this gap, the proposed high-gain single-switch (HGSS) converter combines an LCL-type switched-inductor input network with an enhanced quadratic boost converter (EQBC) and integrates IncCond MPPT. The LCL stage provides source-current conditioning and initial voltage amplification, while the EQBC stage extends the overall gain without extreme duty-cycle operation. The study contributes the hybrid topology, analytical derivation of its operating states, voltage gain and semiconductor stress, and a comparative simulation against a conventional boost converter under the same IncCond strategy: i) Section 2 presents the topology and operating principle; ii) Section 3 describes the MPPT and voltage-control scheme; iii) Section 4 discusses the performance evaluation; and iv) Section 5 concludes the paper.

2. PROPOSED CONVERTER TOPOLOGY AND OPERATING PRINCIPLE

Figure 1 shows the PEMFC interface, in which the HGSS converter raises the low stack voltage to the DC-load level. The topology combines an LCL-type switched-inductor (LCL-SI) input network and an EQBC driven by one active switch; HGSS is used hereafter for this arrangement. The input and output decoupling capacitors C_{FC} and C_{DC} provide local energy buffering and reduce the propagation of switching components between the source, converter, and load. The IncCond loop measures the fuel-cell voltage and current and supplies the duty-cycle command used by the pulse width modulation (PWM) stage. The following subsections first summarize the limitations of the conventional boost converter and then describe the HGSS operating states and gain mechanism.

2.1. Limitations of the conventional boost converter

The conventional boost converter (CBC) has long served as a fundamental topology for DC–DC step-up applications due to its simple structure, which consists of a single input inductor L, an active power switch S, a diode D, and an output filter capacitor C_o, as illustrated in Figure 2. Under ideal operating conditions in continuous conduction mode (CCM), the voltage conversion characteristic of the CBC can be derived by applying the volt–second balance principle to the input inductor over one switching period T_s, which yields.

$$V_{in}DT_s + (V_{in} - V_o)(1 - D)T_s = 0 \quad (1)$$

From this relationship, the static voltage gain of the conventional boost converter is obtained as (2):

$$M_{\text{CBC}} = \frac{V_o}{V_{in}} = \frac{1}{1-D} \quad (2)$$

where $D \in (0,1)$ denotes the duty cycle of the switching signal.

From a purely theoretical standpoint, the above expression implies that the output voltage can be increased indefinitely as the duty cycle approaches unity. In practical implementations, however, particularly in low-voltage renewable energy systems such as photovoltaic arrays or fuel cell stacks, the CBC exhibits several critical limitations when operated at high step-up ratios.

i) Efficiency degradation due to parasitic elements: When the converter operates at extreme duty ratios ($D \to 1$), both the average and peak currents flowing through the inductor, semiconductor switch, and diode increase significantly. Under these conditions, parasitic resistances, including the inductor winding resistance R_L, capacitor equivalent series resistance (ESR), and the MOSFET on-state resistance $R_{\text{DS(on)}}$ give rise to substantial conduction losses. As a result, the overall conversion efficiency deteriorates rapidly beyond a certain duty cycle, even though the theoretical voltage gain continues to increase.

ii) Reverse recovery effects and electromagnetic interference: At high switching frequencies, the output diode of the CBC is subjected to severe reverse recovery stress, leading to additional switching losses and pronounced electromagnetic interference (EMI). These effects degrade power quality and complicate electromagnetic compatibility (EMC) compliance, especially in high-gain operating conditions.

iii) Practical limitation of achievable voltage gain: When conduction losses and parasitic components are taken into account, the effective voltage gain of the CBC saturates well below its theoretical limit. Consequently, increasing the duty cycle beyond a certain threshold fails to deliver the desired output voltage and may even compromise system stability.

iv) High voltage and current stress on semiconductor devices: In the classical boost topology, the voltage stress across both the main switch and the output diode is approximately equal to the output voltage V_o. Therefore, applications requiring high output voltage necessitate the use of high-voltage-rated semiconductor devices, which typically exhibit higher conduction resistance and increased losses. Moreover, elevated peak currents exacerbate thermal stress, imposing stringent cooling requirements and reducing long-term system reliability.

v) Large input current ripple: Although the input inductor enables CCM operation, the source-side current of the CBC still exhibits considerable ripple when the converter operates at high duty ratios. This characteristic is particularly undesirable for sensitive energy sources such as photovoltaic modules and fuel cells, where excessive current ripple can reduce energy extraction efficiency and accelerate source aging.

The aforementioned physical and operational constraints clearly indicate that relying on extreme duty cycle operation in conventional boost converters is not a viable solution for high step-up voltage applications. These limitations have motivated the development of advanced non-isolated converter topologies that integrate gain-extension techniques such as voltage multiplier cells (VMCs) and switched-inductor (SI) networks. Such approaches enable significantly higher voltage gain at moderate duty ratios while preserving the structural simplicity inherent to single-switch converter architectures.

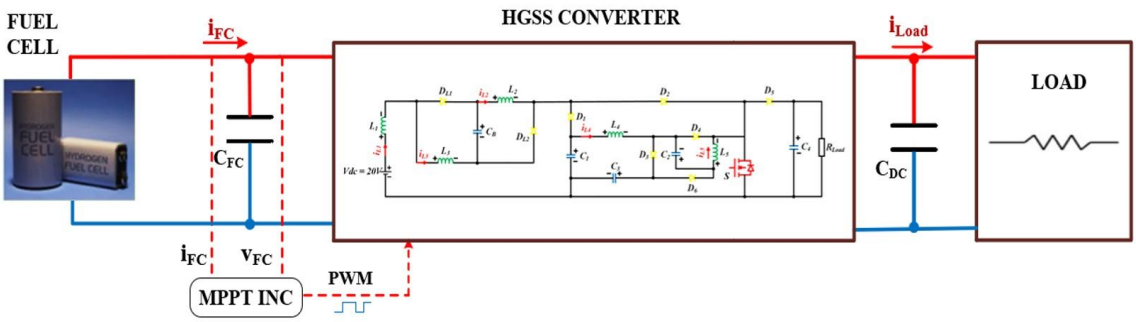

Figure 1. Overall configuration of the proposed fuel cell energy conversion system employing the HGSS converter with IncCond MPPT

2.2. Ultra-high step-Up single-switch DC–DC converter based on hybrid LCL-SI and EQBC structures

To address the physical limitations of the conventional boost converter discussed earlier, this work introduces a hybrid power conversion topology. The proposed HGSS converter integrates an extended LCL-type switched-inductor network at the input stage with an EQBC structure at the output stage. The detailed circuit configuration of the proposed HGSS converter is shown in Figure 3.

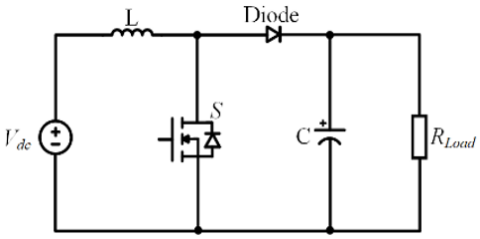

Figure 2. Circuit configuration of the conventional boost converter

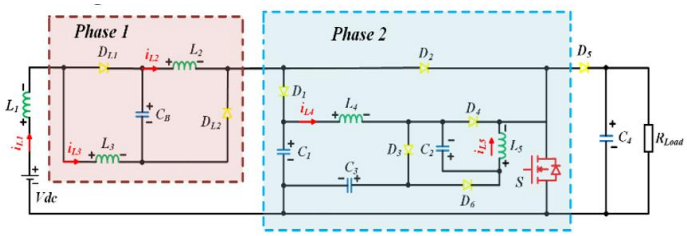

Figure 3. Circuit configuration of the proposed HGSS converter based on the hybrid LCL-SI/EQBC topology

2.2.1. Circuit structure analysis

Referring to Figure 3, the proposed HGSS converter is organized as two cascaded energy conversion stages controlled by a single active power switch S. Input filtering stage: At the input terminal of the converter, an inductor L_1 is connected in series with the source. Its primary function is to smooth the input current and suppress current ripple to a minimum level. This feature is particularly important for sensitive energy sources such as fuel cells, as it helps extend source lifetime and prevents high-frequency switching disturbances generated by the LCL network from propagating back to the source.

Phase 1 - Switched LCL network: The first energy conversion stage consists of two inductors L_2 and L_3, an intermediate capacitor C_B, and guiding diodes D_{L1} and D_{L2}. This stage operates as the main pre-amplification unit of the converter. Through appropriate diode orientation, the inductors are charged in parallel and discharged in series during a switching cycle, enabling an inherent voltage gain at the input stage without increasing the current stress on the main power switch.

Phase 2 - EQBC with integrated VMC: Downstream of the DC-link capacitor C_1, an EQBC combined with a VMC is employed. This stage comprises inductors L_4 and L_5, pumping capacitors C_2 and C_3, and diodes D_1, D_2, D_3, D_4, and D_6. The DC-link capacitor C_1 behaves as a stiff voltage source, isolating disturbances from the input stage while supplying stable energy to the subsequent gain-extension stage.

2.2.2. Operating principle

The operating principle of the proposed HGSS converter is analyzed under CCM. For the analytical derivation, semiconductor voltage drops and the impedance of the input filter inductor L_1 are neglected. These assumptions simplify the gain derivation and do not constitute a device-level loss model. Within one switching period T_s, operation is divided into two states.

State 1 - Magnetization Phase (Switch ON): When the power switch S is turned ON, a closed current path to ground is established. In Phase 1, the source current, after being smoothed by the input inductor L_1, is split to simultaneously charge inductors L_2 and L_3. The current circulates through the guiding diodes D_{L1}, D_{L2}, and the interstage diode D_2. During this interval, the buffer capacitor C_B participates in the conduction loop, clamping the voltages across L_2 and L_3 to approximately the input voltage. In Phase 2, the energy stored in the DC-link capacitor C_1 is released to magnetize inductor L_4 through diode D_4 and the active switch S. In parallel, the pumping capacitor C_2 forward-biases diode D_6, transferring its stored energy to inductor L_5. During this state, the output diode D_5 is reverse-biased due to a higher potential at its cathode, thereby isolating the load from the source. The load demand is fully supported by the output capacitor C_4.

State 2 - Energy Transfer Phase (Switch OFF): When the power switch S is turned OFF, the magnetic energy stored in the inductor's collapses, generating large induced electromotive forces. In Phase 1, the induced voltages across inductors L_2 and L_3 forward-bias diode D_1. Consequently, the energy stored in L_2, L_3, and the buffer capacitor C_B is released in series to strongly charge the DC-link capacitor C_1. Simultaneously, due to the change in node voltages, the input diodes D_{L1} and D_{L2} become reverse-biased and cease conduction. In Phase 2, the induced voltage across inductor L_4 forward-biases diode D_3, allowing its stored magnetic energy to be transferred to capacitor C_3. At the output branch, owing to the electromagnetic

inertia of inductor L_5, diode D_5 becomes forward-biased. The combined energy from capacitor C_2 and inductor L_5 is then delivered to charge the output capacitor C_4 and supply the load. During this interval, diodes D_2 and D_4 are reverse-biased.

2.2.3. Quantitative analysis of the voltage conversion ratio

Under steady-state conditions, the HGSS voltage gain is derived using volt–second balance. The converter is treated as two cascaded gain stages so that the contribution of each stage is explicit. Phase 1 (LCL network): Inductors L_2 and L_3 are charged in parallel and discharged in series through the intermediate capacitor C_{B}. The resulting DC-link voltage V_{C1} is obtained from the volt–second balance condition:

$$V_{L2,\mathrm{ON}} \cdot D + V_{L2,\mathrm{OFF}} \cdot (1 - D) = 0 \tag{3}$$

Accordingly, the voltage gain of the first stage is obtained as (4).

$$G_{\mathrm{LCL}} = \frac{V_{C1}}{V_{in}} = \frac{2}{1-D} \tag{4}$$

This expression indicates that, even at the initial conversion stage, the proposed LCL network doubles the voltage gain of a conventional boost converter operating at the same duty cycle. Voltage gains of phase 2 (EQBC–VMC Network): The second stage integrates the EQBC with a VMC. This stage is driven by the intermediate DC-link voltage V_{C1}, obtained from the preceding LCL stage, and performs the final voltage step-up to the output voltage V_o. By applying energy balance principles to the inductor L_4 and pumping capacitor C_2, the voltage conversion relationship of this stage is derived as (5).

$$G_{\mathrm{EQBC}} = \frac{V_o}{V_{C1}} = \frac{2-D}{(1-D)^2} \tag{5}$$

Overall voltage conversion ratio: The overall voltage gain of the proposed system, denoted as M, is obtained as the product of the gains of the two cascaded stages. By combining G_{LCL} and G_{EQBC}, the overall voltage conversion ratio is expressed as (6).

$$M = \frac{V_o}{V_{in}} = G_{\mathrm{LCL}} \cdot G_{\mathrm{EQBC}} = \left(\frac{2}{1-D}\right)\left(\frac{2-D}{(1-D)^2}\right) \tag{6}$$

After simplification, the final analytical expression of the voltage gain is given by (7).

$$M = \frac{2(2-D)}{(1-D)^3} \tag{7}$$

The (7) confirms that the proposed converter exhibits a cubic voltage step-up characteristic. This feature provides a significant advantage over conventional first- and second-order boost structures, as it enables extremely high voltage conversion ratios at moderate duty cycles. For instance, a gain of $M = 20$ can be achieved at $D = 0.475$ without approaching the physical limitations associated with extreme duty cycle operation of the power switch.

2.2.4. Component stress analysis and input current characteristics

Semiconductor stress is examined to identify the device requirements of the HGSS converter. The analytical expressions show how voltage is distributed across the switch and diodes; any reduction in device rating, conduction loss, or cost must still be verified using the selected components and their parasitic parameters.

i) Voltage stress on semiconductor devices: A key advantage of the proposed hybrid structure lies in the significant reduction of voltage stress across the diodes, particularly those located in the input-stage LCL network (Phase 1). Diodes in the LCL network (D_{L1}, D_{L2}): Owing to their placement in the low-voltage region of the converter, the reverse voltage stress experienced by these diodes represents only a small fraction of the output voltage. Specifically, the maximum voltage stress can be expressed as (8).

$$V_{D_{L1}} = V_{D_{L2}} = \frac{(1-D)^2}{2(2-D)} V_o \tag{8}$$

The (8) shows that the input-stage diode stress decreases as the duty ratio increases. This may permit lower-voltage Schottky devices in the LCL branch, although practical loss depends on their forward drop and current rating. For the main switch S_1, the voltage stress is approximately equal to the output voltage ($(V_{S1} \approx V_o)$). The corresponding current and thermal margins must therefore be checked against the selected device ratings.

ii) Input current ripple and source protection: Current ripple is relevant to PEMFC durability because large pulsating components can interact with the stack electrochemical and thermal dynamics. The series input inductor L_1 provides a continuous current path and attenuates switching-frequency ripple before it reaches the source. The present simulations quantify output-voltage and output-current ripple rather than source-current ripple; therefore, the source-side benefit should be confirmed experimentally.

3. MPPT IMPLEMENTATION AND CONTROL STRATEGY

Although the perturb and observe (P&O) algorithm is widely adopted due to its simplicity, it inherently suffers from continuous oscillations around the MPP and may lose tracking accuracy under rapidly changing operating conditions. To overcome these dynamic limitations, this study employs the incremental conductance (IncCond) strategy, which exploits the derivative characteristics of the fuel cell power–voltage curve. The fundamental principle of the IncCond method is based on the fact that the slope of the power–voltage curve becomes exactly zero at the MPP. The derivative of the output power with respect to voltage can be expressed as (9).

$$\frac{dP}{dV} = \frac{d(IV)}{dV} = I + V\frac{dI}{dV} \tag{9}$$

At the MPP, this derivative equals zero, yielding the equilibrium condition.

$$I + V\frac{dI}{dV} = 0 \quad \Rightarrow \quad \frac{dI}{dV} \approx -\frac{I}{V} \tag{10}$$

Here, I/V is the instantaneous conductance and dI/dV is the incremental conductance. Their relationship identifies the direction of the operating point relative to the MPP and determines the duty-cycle update D. When the incremental condition is satisfied, the implementation holds the duty command rather than applying another perturbation. Figure 4 shows the implemented flowchart. At each sampling instant k, the controller measures the fuel cell current $I(k)$ and voltage $V(k)$, and computes the incremental variations ΔI and ΔV. The duty-cycle update law for the boost-based HGSS converter, which exhibits an inverse input-voltage characteristic (i.e., increasing D reduces the input voltage), is determined according to the following cases.

3.1. Case 1

Voltage variation ($\Delta V \neq 0$). If $\frac{\Delta I}{\Delta V} > -\frac{I}{V}$, the operating point lies to the left of the MPP, corresponding to a positive slope of the power–voltage curve. To move toward the maximum power point, the fuel cell voltage V_{fc} must be increased. Due to the inverse characteristic of the boost converter, the duty cycle is therefore reduced as $D(k) = D(k-1) - \Delta D$. If $\frac{\Delta I}{\Delta V} < -\frac{I}{V}$, the operating point is located to the right of the MPP, where the slope of the power–voltage curve is negative. In this case, the fuel cell voltage must be decreased, which is achieved by increasing the duty cycle $D(k) = D(k-1) + \Delta D$. If $\frac{\Delta I}{\Delta V} = -\frac{I}{V}$, the system operates exactly at the MPP. The duty cycle is therefore held constant, $D(k) = D(k-1)$, which avoids an additional duty perturbation at that sampling instant.

3.2. Case 2

No voltage variation ($\Delta V = 0$). This special case occurs when environmental conditions change rapidly while the voltage has not yet responded. The control decision is then based on the current variation: If $\Delta I > 0$, the output power is increasing, and the controller continues adjusting in the direction that increases the fuel cell voltage, yielding $D(k) = D(k-1) - \Delta D$. If $\Delta I < 0$, the output power decreases, and the duty cycle is adjusted in the opposite direction, given by $D(k) = D(k-1) + \Delta D$.

In addition to the IncCond duty update, the simulation model includes a digital proportional–integral (PI) term for DC-bus regulation. The voltage error is defined as $e(k) = V_{\text{ref}} - V_o(k)$, and the PI output follows the discrete-time law.

$$u(k) = K_p e(k) + K_i \sum e\,(k) T_s \tag{11}$$

where K_p and K_i denote the proportional and integral gains, respectively.

A soft-start limit is applied to reduce inrush current. The duty cycle is restricted to approximately $D \approx 0.3$ during the initial interval $t < 0.18\ s$, after which the model transitions to its closed-loop operating mode. Under the tested conditions, the IncCond update and PI feedback produce the responses reported in section 4. The IncCond logic reduces repeated perturbation near $\frac{dP}{dV} = 0$, but tracking performance remains dependent on the sampling interval, duty-step size, measurement quality, and interaction with the voltage-regulation loop.

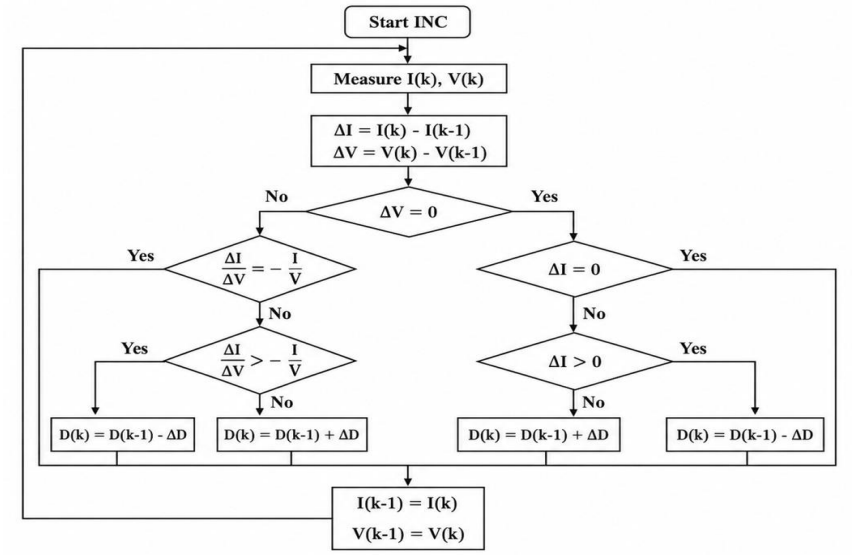

Figure 4. Flowchart of the IncCond MPPT algorithm

4. SIMULATION AND PERFORMANCE EVALUATION

A MATLAB/Simulink model was used to evaluate the proposed HGSS converter with the incremental conductance (IncCond) MPPT algorithm. The study examines voltage step-up, transient response, and model-based conversion efficiency for the low-voltage PEMFC source. The source is represented by the PEMFC – 1.26 kW – 24 Vdc block in Simplified mode. At nominal operation, it supplies 52 A at 24.23 V (approximately 1.26 kW); its open-circuit voltage is 42 V, falling to 24.23 V at nominal load and to about 20 V at 100 A. This 20–42 V range and the associated voltage sag provide the test conditions for regulation of a high-voltage DC bus. The HGSS model is evaluated for conversion to the 300 V target and for attenuation of source-side switching components through the input filtering stage. Figure 5 shows the complete simulation schematic. The HGSS and conventional boost converter models were compared using the same IncCond MPPT strategy, fuel-cell source, 50 kHz switching frequency, 90 Ω resistive load, and startup from rest at $t = 0$. Figure 6 reports the output voltage, output current, output power, and duty cycle for this common test condition.

Figure 6 compares the dynamic performance of the proposed HGSS converter with that of the conventional boost converter under identical operating conditions. The proposed converter rapidly reaches steady state and regulates the output voltage at approximately 300 V, whereas the conventional converter exhibits pronounced oscillations and maintains only about 260–270 V. Correspondingly, the HGSS converter supplies approximately 3.3 A and 1 kW to the load, compared with 2.8–3.0 A and about 800 W for the conventional topology. Thus, the proposed converter delivers approximately 25% more output power. This improvement is mainly attributed to its higher intrinsic voltage gain: the HGSS converter operates at a moderate duty cycle of approximately 0.52, while the conventional converter approaches duty-cycle saturation at approximately 0.9. The lower duty cycle provides a wider control margin and reduces the adverse effects associated with extreme-duty-cycle operation. The steady-state voltage and current ripples were further evaluated over the interval from 0.5 to 2 s using RMS and peak-to-peak percentage indices, as presented in Figure 7. As shown in Figure 7, the proposed HGSS converter substantially improves steady-state output quality. The RMS ripple of both the output voltage and load current decreases from 3.26% to 0.48%, corresponding to an 85.3% reduction. Similarly, the peak-to-peak ripple decreases from 21.54% to 3.22%, representing an 85.1% reduction. These results demonstrate that the hybrid LCL-SI/EQBC topology provides tighter voltage regulation and smoother load-current delivery than the conventional boost converter.

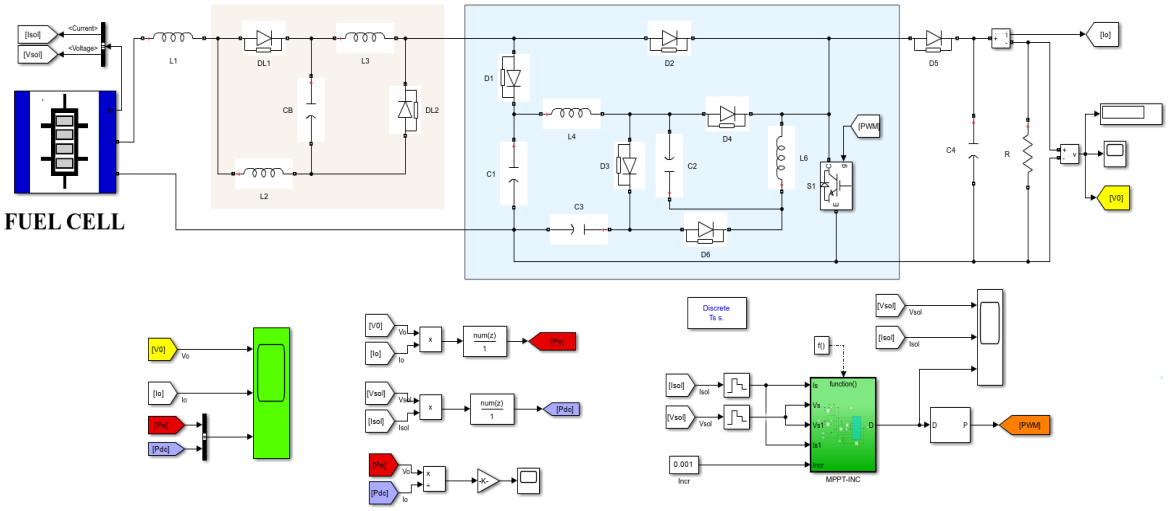

Figure 5. MATLAB/Simulink simulation model of the PEM fuel cell system employing the proposed HGSS converter based on the hybrid LCL-SI/EQBC topology with IncCond MPPT control

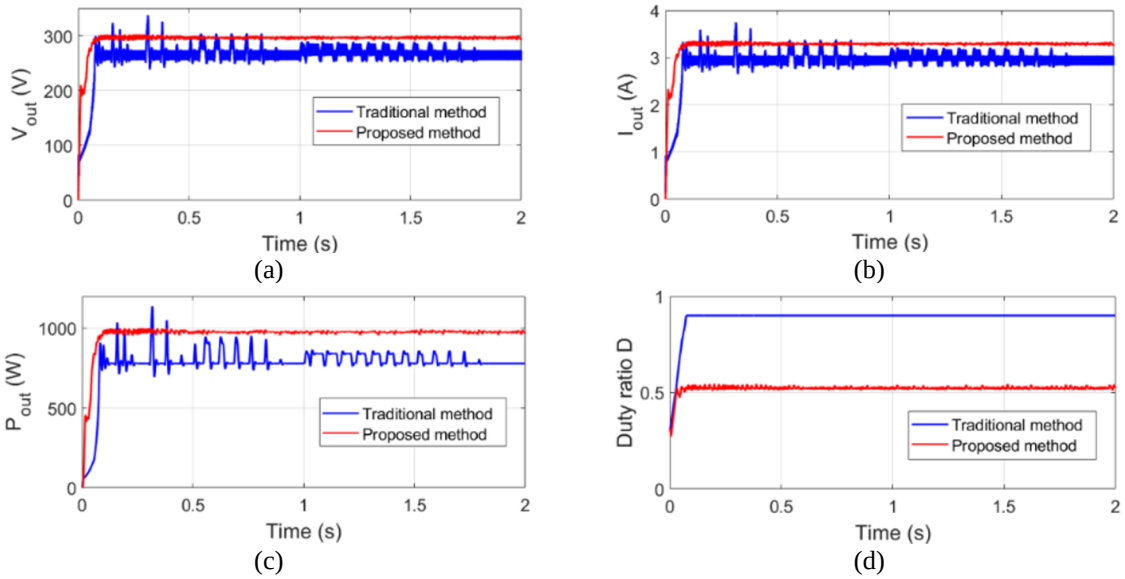

Figure 6. Performance comparison between the proposed HGSS converter and the conventional boost converter with IncCond MPPT under a 90 Ω load: (a) output voltage, (b) output current, (c) output power, and (d) duty cycle

Figure 8 shows that the input and output powers settle after approximately 0.2 s. The fuel cell supplies about 1.25 kW, while the converter delivers approximately 1 kW to the load, giving a simulated steady-state efficiency of 78–82% for a voltage conversion ratio above 12. Because the analytical model neglects device drops and the study does not report a separate parasitic or thermal loss breakdown, this efficiency should be interpreted as a model-specific simulation result rather than experimentally verified converter efficiency.

Within the simulated conditions, the HGSS converter provides a higher regulated voltage and output power, lower output ripple, and a lower duty cycle than the conventional boost baseline. These benefits require additional inductors, capacitors, and diodes, which increase passive volume, implementation complexity, and potential conduction loss. The present study is simulation-based and does not quantify device-level thermal behavior, lifetime, or hardware cost; experimental validation is therefore required before conclusions are drawn about practical reliability or cost-effectiveness.

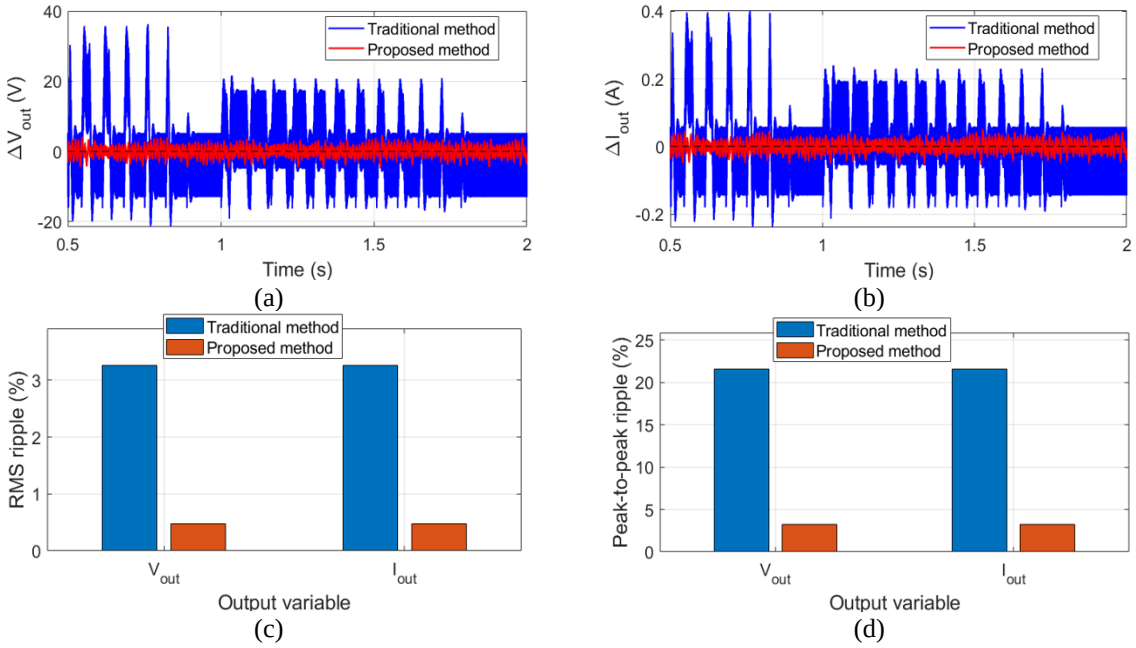

Figure 7. Steady-state ripple comparison between the conventional boost converter and the proposed HGSS converter under a 90 Ω load over 0.5–2.0 s: (a) output-voltage ripple, (b) output-current ripple, (c) RMS ripple percentage, and (d) peak-to-peak ripple percentage

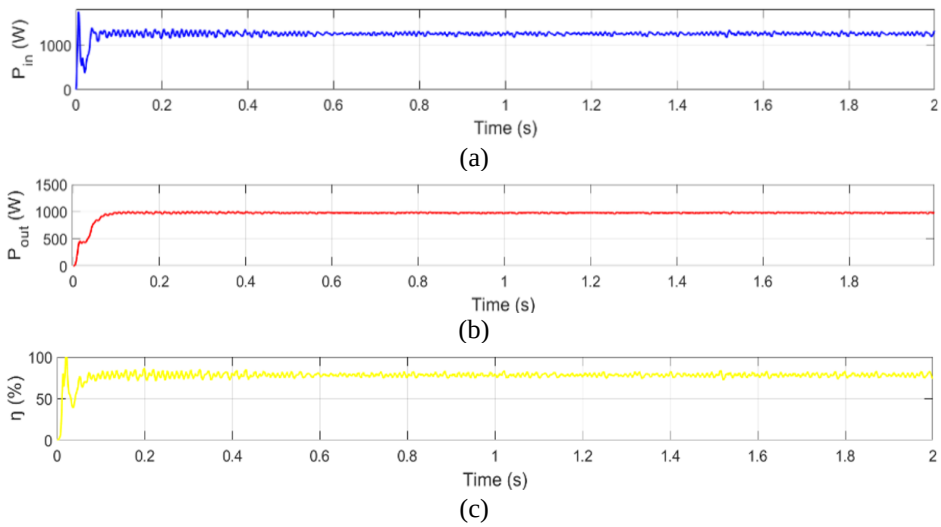

Figure 8. Energy characteristics of the proposed HGSS converter under nominal operating conditions: (a) fuel-cell input power, (b) output power, and (c) instantaneous conversion efficiency

5. CONCLUSION

An HGSS conversion framework combining a single-switch LCL-SI/EQBC topology with IncCond MPPT was evaluated for PEMFC applications. For the 1.26 kW PEMFC model, the converter raised the input voltage from 20 V to a regulated 300 V at approximately 80% simulated efficiency. Under the same MPPT and load conditions, it delivered about 25% more output power than the conventional boost converter, reduced RMS and peak-to-peak output ripple by approximately 85%, and operated at a duty cycle of 0.52 instead of 0.9. The comparison is limited to MATLAB/Simulink and a conventional boost baseline; source-current ripple, device parasitics, thermal behavior, and hardware operation remain to be verified. Future work will therefore address prototype validation, loss-oriented design, and tests under dynamic source and load conditions.

FUNDING INFORMATION

Authors state no funding involved.

AUTHOR CONTRIBUTIONS STATEMENT

This journal uses the Contributor Roles Taxonomy (CRediT) to recognize individual author contributions, reduce authorship disputes, and facilitate collaboration.

Name of Author	C	M	So	Va	Fo	I	R	D	O	E	Vi	Su	P	Fu
Thanh-Lam Le	✓	✓	✓	✓	✓	✓	✓	✓	✓	✓	✓	✓	✓	✓
Nguyen Thi Bich Mai			✓			✓		✓	✓		✓			✓

C : **C**onceptualization
M : **M**ethodology
So : **So**ftware
Va : **Va**lidation
Fo : **Fo**rmal analysis
I : **I**nvestigation
R : **R**esources
D : **D**ata Curation
O : Writing - **O**riginal Draft
E : Writing - Review & **E**diting
Vi : **Vi**sualization
Su : **Su**pervision
P : **P**roject administration
Fu : **Fu**nding acquisition

CONFLICT OF INTEREST STATEMENT

Authors state no conflict of interest.

DATA AVAILABILITY

Data availability is not applicable to this paper as no new data were created or analyzed in this study.

REFERENCES

[1] W. S. Ebhota and T.-C. Jen, "Fossil fuels environmental challenges and the role of solar photovoltaic technology advances in fast tracking hybrid renewable energy system," *International Journal of Precision Engineering and Manufacturing-Green Technology*, vol. 7, no. 1, pp. 97–117, Jan. 2020, doi: 10.1007/s40684-019-00101-9.

[2] S. Yi, K. Raza Abbasi, K. Hussain, A. Albaker, and R. Alvarado, "Environmental concerns in the United States: Can renewable energy, fossil fuel energy, and natural resources depletion help?," *Gondwana Research*, vol. 117, pp. 41–55, May 2023, doi: 10.1016/j.gr.2022.12.021.

[3] S. Mo *et al.*, "Recent advances on PEM fuel cells: from key materials to membrane electrode assembly," *Electrochemical Energy Reviews*, vol. 6, no. 1, Dec. 2023, doi: 10.1007/s41918-023-00190-w.

[4] X. Wu, J. Wang, Y. Zhang, J. Du, Z. Liu, and Y. Chen, "Review of DC-DC converter topologies based on impedance network with wide input voltage range and high gain for fuel cell vehicles," *Automotive Innovation*, vol. 4, no. 4, pp. 351–372, Nov. 2021, doi: 10.1007/s42154-021-00163-z.

[5] Y. Huangfu, Y. Ma, H. Bai, L. Xu, A. Wang, and R. Ma, "A family of high gain fuel cell front-end converters with low input current ripple for PEMFC power conditioning systems," *International Journal of Hydrogen Energy*, vol. 46, no. 53, pp. 27156–27172, Aug. 2021, doi: 10.1016/j.ijhydene.2021.05.174.

[6] P. Thounthong, S. Raël, and B. Davat, "Energy management of fuel cell/battery/supercapacitor hybrid power source for vehicle applications," *Journal of Power Sources*, vol. 193, no. 1, pp. 376–385, Aug. 2009, doi: 10.1016/j.jpowsour.2008.12.120.

[7] O. P. Jaga, R. Gupta, B. Jena, and S. G. Choudhuri, "Bi-directional DC/DC converters used in interfacing ESSs for RESs and EVs: a review," *IETE Technical Review*, vol. 40, no. 3, pp. 334–370, May 2023, doi: 10.1080/02564602.2022.2116362.

[8] I. K. Denholm, W. Hassan, M. Negnevitsky, and D. D.-C. Lu, "Optimized interleaved ultra-high gain DC-DC power converter with low ripple input current and voltage stress for fuel cell systems," *IEEE Access*, vol. 12, pp. 121052–121063, 2024, doi: 10.1109/ACCESS.2024.3450887.

[9] M. Forouzesh, Y. P. Siwakoti, S. A. Gorji, F. Blaabjerg, and B. Lehman, "Step-up DC–DC converters: a comprehensive review of voltage-boosting techniques, topologies, and applications," *IEEE Transactions on Power Electronics*, vol. 32, no. 12, pp. 9143–9178, Dec. 2017, doi: 10.1109/TPEL.2017.2652318.

[10] H. Meshael, A. Elkhateb, and R. Best, "Topologies and design characteristics of isolated high step-Up DC–DC converters for photovoltaic systems," *Electronics*, vol. 12, no. 18, Sep. 2023, doi: 10.3390/electronics12183913.

[11] I. Alhurayyis, A. Elkhateb, and J. Morrow, "Isolated and nonisolated DC-to-DC converters for medium-voltage DC networks: a review," *IEEE Journal of Emerging and Selected Topics in Power Electronics*, vol. 9, no. 6, pp. 7486–7500, Dec. 2021, doi: 10.1109/JESTPE.2020.3028057.

[12] A. Gupta, N. Korada, and R. Ayyanar, "Quadratic-extended-duty-ratio boost converters for ultra high gain application with low input current ripple and low device stress," *IEEE Transactions on Industry Applications*, vol. 59, no. 1, pp. 938–948, Jan. 2023, doi: 10.1109/TIA.2022.3207132.

[13] T.-L. Le, L. Van Truc, and T. N. Tien, "Cascaded PI-controlled multistage boost converter for low-voltage renewable sources," *Engineering, Technology & Applied Science Research*, vol. 15, no. 5, pp. 26777–26782, Oct. 2025, doi: 10.48084/etasr.12941.

[14] A. Alkhaldi, A. Elkhateb, and D. Laverty, "Voltage lifting techniques for non-isolated DC/DC converters," *Electronics*, vol. 12, no. 3, Feb. 2023, doi: 10.3390/electronics12030718.

[15] T. Kobaku, R. Jeyasenthil, S. Sahoo, R. Ramchand, and T. Dragicevic, "Quantitative feedback design-based robust PID control of voltage mode controlled DC-DC boost converter," *IEEE Transactions on Circuits and Systems II: Express Briefs*, vol. 68, no. 1, pp. 286–290, Jan. 2021, doi: 10.1109/TCSII.2020.2988319.

[16] H. Wang, Y. Dong, G. He, and W. Song, "Fixed-time backstepping sliding-mode control for interleaved boost converter in DC microgrids," *Energies*, vol. 17, no. 21, Oct. 2024, doi: 10.3390/en17215377.
[17] A. Kulshreshtha, A. R. Saxena, and M. Veerachary, "Non-isolated fourth-order boost DC-DC converter for power management in low voltage low power DC Grids: design and interaction analysis," *IEEE Access*, vol. 8, pp. 196500–196514, 2020, doi: 10.1109/ACCESS.2020.3034181.
[18] A. Rajamallaiah *et al.*, "Deep reinforcement learning for power converter control: a comprehensive review of applications and challenges," *IEEE Open Journal of Power Electronics*, pp. 1–35, 2025, doi: 10.1109/OJPEL.2025.3619673.
[19] R. S. Gemmen, "Analysis for the effect of inverter ripple current on fuel cell operating condition," *Journal of Fluids Engineering*, vol. 125, no. 3, pp. 576–585, May 2003, doi: 10.1115/1.1567307.
[20] T. Jarry *et al.*, "Impact of high frequency current ripples on the degradation of high-temperature PEM fuel cells (HT-PEMFC)," *International Journal of Hydrogen Energy*, vol. 48, no. 54, pp. 20734–20742, Jun. 2023, doi: 10.1016/j.ijhydene.2023.03.027.
[21] N. F. N. Ismail, N. Abd. Rahim, S. R. S. Raihan, and Y. Al-Turki, "Parallel inductor multilevel current source inverter for input ripple current reduction in PEM fuel cell applications," *IETE Journal of Research*, vol. 66, no. 4, pp. 505–517, Jul. 2020, doi: 10.1080/03772063.2018.1504699.
[22] Ö. Çelik, "Data-driven MPPT techniques for optimizing vehicular fuel cell performance in hybrid DC microgrid," *International Journal of Hydrogen Energy*, vol. 79, pp. 715–727, Aug. 2024, doi: 10.1016/j.ijhydene.2024.07.033.
[23] V. Prashanth *et al.*, "Implementation of high step-up power converter for fuel cell application with hybrid MPPT controller," *Scientific Reports*, vol. 14, no. 1, Feb. 2024, doi: 10.1038/s41598-024-53763-0.
[24] A. Fathy, H. Rezk, and T. M. Alanazi, "Recent approach of forensic-based investigation algorithm for optimizing fractional order PID-based MPPT with proton exchange membrane fuel cell," *IEEE Access*, vol. 9, pp. 18974–18992, 2021, doi: 10.1109/ACCESS.2021.3054552.
[25] A. M. A. Malkawi *et al.*, "Maximum power point tracking enhancement for PV in microgrids systems using dual artificial neural networks to estimate solar irradiance and temperature," *Results in Engineering*, vol. 25, Mar. 2025, doi: 10.1016/j.rineng.2025.104275.
[26] S. Sarwar *et al.*, "A novel hybrid MPPT Technique to maximize power harvesting from PV system under partial and complex partial shading," *Applied Sciences*, vol. 12, no. 2, Jan. 2022, doi: 10.3390/app12020587.
[27] S. Bhattacharyya, D. S. Kumar P, S. Samanta, and S. Mishra, "Steady output and fast tracking MPPT (SOFT-MPPT) for P& O and InC algorithms," *IEEE Transactions on Sustainable Energy*, vol. 12, no. 1, pp. 293–302, Jan. 2021, doi: 10.1109/TSTE.2020.2991768.
[28] M. Büyük and M. İnci, "Improved drift-free P&O MPPT method to enhance energy harvesting capability for dynamic operating conditions of fuel cells," *Energy*, vol. 267, Mar. 2023, doi: 10.1016/j.energy.2022.126543.
[29] A. Chellakhi, S. El Beid, Y. Abouelmahjoub, and H. Doubabi, "An enhanced incremental conductance MPPT approach for PV power optimization: a simulation and experimental study," *Arabian Journal for Science and Engineering*, vol. 49, no. 12, pp. 16045–16064, Dec. 2024, doi: 10.1007/s13369-024-08804-1.
[30] F. Usman Khan, M. M. Gulzar, D. Sibtain, H. M. Usman, and A. Hayat, "Variable step size fractional incremental conductance for MPPT under changing atmospheric conditions," *International Journal of Numerical Modelling: Electronic Networks, Devices and Fields*, vol. 33, no. 6, Nov. 2020, doi: 10.1002/jnm.2765.

BIOGRAPHIES OF AUTHORS



Thanh-Lam Le received the M.S. degree in electrical engineering from Ho Chi Minh City University of Technology, Vietnam, and the Ph.D. degree in electrical engineering from National Cheng Kung University, Tainan, Taiwan. He is currently a lecturer with the Faculty of Electrical and Electronics Engineering at Ho Chi Minh City University of Technology and Engineering, Vietnam. His research interests include motor drives, energy conversion systems, advanced control theory, and its applications. He can be contacted at email: lamlethanh@hcmute.edu.vn.



Nguyen Thi Bich Mai received the B.S. and M.S. degrees in electrical engineering from Ho Chi Minh City University of Technology and Education, Vietnam. She is currently a lecturer with the Faculty of Electrical and Electronics Engineering at Ho Chi Minh City University of Technology and Engineering, Vietnam. Her research interests include electrical machine simulation and control, data analysis in electrical apparatus, and intelligent control. She can be contacted at email: tohchuenling@yahoo.com.